Ab initio study of the intrinsic exchange bias at the $SrRuO_3/SrMnO_3$ interface

Shuai Dong,[1,2] Qinfang Zhang,[3,4] Seiji Yunoki,[3,4,5] J.-M. Liu,[2,6] and Elbio Dagotto[7,8]

[1]*Department of Physics, Southeast University, Nanjing 211189, China*
[2]*National Laboratory of Solid State Microstructures, Nanjing University, Nanjing 210093, China*
[3]*Computational Condensed Matter Physics Laboratory, RIKEN, Wako, Saitama 351-0198, Japan*
[4]*CREST, Japan Science and Technology Agency (JST), Kawaguchi, Saitama 332-0012, Japan*
[5]*Computational Materials Science Research Team, RIKEN AICS, Kobe, Hyogo 650-0047, Japan*
[6]*International Center for Materials Physics, Chinese Academy of Sciences, Shenyang 110016, China*
[7]*Department of Physics and Astronomy, University of Tennessee, Knoxville, Tennessee 37996, USA*
[8]*Materials Science and Technology Division, Oak Ridge National Laboratory, Oak Ridge, Tennessee 37831, USA*

(Dated: December 22, 2011)

In a recent publication (S. Dong *et al.*, Phys. Rev. Lett. **103**, 127201 (2009)), two (related) mechanisms were proposed to understand the intrinsic exchange bias present in oxides heterostructures involving G-type antiferromagnetic perovskites. The first mechanism is driven by the Dzyaloshinskii-Moriya interaction, which is a spin-orbit coupling effect. The second is induced by the ferroelectric polarization, and it is only active in heterostructures involving multiferroics. Using the $SrRuO_3/SrMnO_3$ superlattice as a model system, density-functional calculations are here performed to verify the two proposals. This proof-of-principle calculation provides convincing evidence that qualitatively supports both proposals.

PACS numbers: 75.70.Cn, 75.30.Et, 75.80.+q

I. INTRODUCTION

The exchange bias (EB) effect is known to be present in a wide range of magnetic composites. This effect has been extensively used in a variety of magnetic storage and sensor devices.[1–6] In principle, the physical origin of the EB is the magnetic coupling at the interface between antiferromagnetic (AFM) and ferromagnetic (FM) (or ferrimagnetic) materials. However, a more fundamental microscopic theoretical understanding of the subtle EB effect has not been developed in spite of the fact that the EB phenomenon has been known for more than half a century and used in industry for decades. In many textbooks of magnetism, the EB is described as induced by spin pinning effects at the FM/AFM interface. An uncompensated AFM interface, which means there is a net magnetic moment at the interface on the AFM side, is often invoked to illustrate how the pinning may work, as sketched in Fig. 1(a). These uncompensated magnetic moments provide a bias field to the neighboring FM moments via the exchange coupling across the interface. This ideal scenario is very clear with regards to the possible cause of the effect, but it appears incomplete since it actually fails in several real cases.[7]

To understand the deficiencies of the uncompensated AFM scenario, consider the case of AFM interfaces that are optimally uncompensated, as in Fig. 1(a). An example is provided by the (111) surface of G-type AFM materials. In these cases, a large EB would be expected. However, such an effect has not been observed in real materials with these characteristics.[7] In contrast, several *compensated* AFM interfaces, as illustrated in Figs. 1(b) and (c), do display an EB effect, that may be even larger than for the "uncompensated" interface of the same materials.[7] To solve these puzzles, several possible mechanisms have been proposed in the past decades. Extrinsic factors are often considered, such as interface roughness,[8,9] spin canting near the interface,[10] frozen interfacial and domain pinning,[11,12] and others. For more details, the readers are referred to the theoretical review by Kiwi that summarizes several previous models.[7] In most of these models, a small "frozen" uncompensation of the AFM moments near the interface remains the common ingredient for the explanation of the bias field, despite the different origins of this uncompensation.

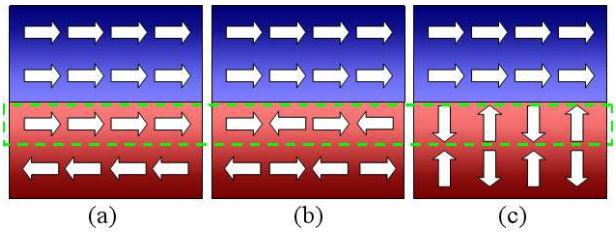

FIG. 1. (Color online) Sketch of possible FM-AFM interfaces. The upper/lower (blue/red) layers denote FM/AFM components, respectively. Local magnetic moments are marked as arrows. (a) A fully uncompensated AFM interface, as it occurs for example in an (001) surface of A-type AFM state or (111) surface of G-type AFM state. (b-c) Fully compensated AFM interfaces, as they occur in a G-type AFM state. In (a) and (b), the FM and AFM magnetic moments are collinear. In (c), the FM and AFM magnetic moments are noncollinear, namely the magnetic easy axes of the FM and AFM materials are different.

In recent years, considerable attention and research have been devoted to the study of the exchange bias in magnetic oxides heterostructures.[13,14] In particular, when a multiferroic material participates as one of the two components at the interface, the exchange bias can

then be tuned by electric fields,[15–21] an effect that is difficult to understand with only purely magnetic arguments. Motivated by these experimental studies, some of the present authors have recently proposed two (related) mechanisms to understand the EB effects in magnetic oxides heterostructures.[22] These mechanisms are based on the Dzyaloshinskii-Moriya (DM) interaction and on the ferroelectric (FE) polarization, with the later only active in the heterostructures that involve multiferroics. These two mechanisms are quite different from previous models used to address the EB effect, since they do not rely on the existence of uncompensated AFM moments anymore.

The DM interaction was first proposed over half a century ago (two years after the observation of the EB effect) to explain the existence of weak ferromagnetism in some AFM materials.[23,24] The DM interaction originates in the spin-orbit coupling (SOC) effect caused by relativistic corrections to superexchange. This DM interaction can be written as $\vec{D}_{ij} \cdot (\vec{S}_i \times \vec{S}_j)$, where $\vec{S}_i$ and $\vec{S}_j$ are nearest-neighbor spins. The vector $\vec{D}_{ij}$ obeys the asymmetric rule $\vec{D}_{ij} = -\vec{D}_{ji}$. In transitional metal oxides, $\vec{D}_{ij}$ is determined by the bending of the M_i-O-M_j bond (where M's denote transition metal ions and O the oxygen ion). From symmetry considerations, the direction of $\vec{D}_{ij}$ should be perpendicular to the plane spanned by the bended M_i-O-M_j bond.[24] The intensity of $|\vec{D}_{ij}|$ is proportional to the oxygen displacements from the middle point of M_i-M_j.[25] Thus, if the M_i-O-M_j bond is straight, namely a 180° angle bond, then $\vec{D}_{ij}$ becomes zero.

According to the formula for the DM interaction, the presence of a non-collinear spin pair is a key ingredient.However, these spin arrangements are not very common as ground states in bulk materials since most spin states are typically governed by strong superexchange interactions that often favor collinear states. However, it is quite natural to have noncollinear spin pairs across the interfaces in heterostructures, due to the different magnetic easy axes of the two components.

In bulks of several perovskites, there are intrinsic and collective tiltings and rotations of the oxygen octahedra, which are often generically called the "$GdFeO_3$-type" distortions.[26] In several oxide thin films and heterostructures these octahedral tiltings and rotations are still present, although the distortion modes may change with respect to those that exist in the bulk limit due to the lattice mismatch and substrate strain or stress.[27–30] A crucial aspect of our arguments is that due to these collective octahedral distortions, the M_i-O-M_j bonds are bent in a *staggered* manner, giving rise to the staggered arrangement of $\vec{D}$ vectors shown in Fig. 2 (b). According to our recent model investigations, a uniform bias field emerges from the combination of the staggered $\vec{D}$ vectors and the staggered G-type AFM spin order.[22]

Furthermore, if one component has an (in-plane) FE polarization which induces a uniform displacement between cations and anions, the angles of the M_i-O-M_j bonds become staggered, as sketched in Figs. 2(b) and (c). As a result, the intensities of the exchange couplings are modulated, which also induces a uniform bias field when in the presence of the G-type AFM spin order.[22]

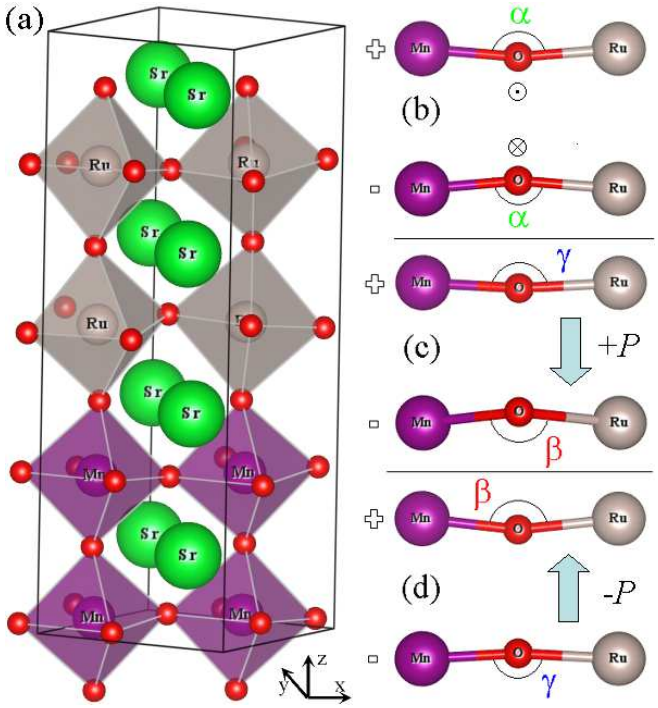

FIG. 2. (Color online) (a) Optimized superlattice crystal structure (drawn by VESTA).[31] The space group is $Pmc2_1$ (orthorhombic). The in-plane lattice constants a and b are fixed as $3.905\sqrt{2}$ Å to match the $SrTiO_3$ substrate. The optimized c-axis constant is 15.5 Å. The pseudo-cubic x-y-z axes are shown. The collective rotations/tiltings of oxygen octahedra are obvious to the eye, giving rise to bended Mn-O-Mn, Mn-O-Ru, and Ru-O-Ru bonds. (b) The optimized Mn-O-Ru bond angles α are 170.4°, while the bending directions between nearest-neighbor pairs are staggered. The $\vec{D}$'s point "in" ($\odot$) and "out" ($\otimes$) for these two bonds respectively. (c-d): When an (in-plane) FE polarization $\vec{P}$ (the interfacial oxygens displaced along the [110] direction by $0.005\sqrt{2}$ Å) is imposed to the original bending bonds, then the bond angles become modulated: β=168.5° and γ=171.6°. Here the difference between β and γ is enlarged for a better visual comparison.

Therefore, these two mechanisms rely on the crystal distortions, the spin-orbit coupling, and the spin-lattice coupling, all of which are *intrinsic* in oxide heterostructures. However, from the experimental information available up to date it remains difficult to reach a definitive conclusion about the validity of the proposed mechanisms, particularly considering the complexity of real oxide heterostructures. Thus, it is very important to analyze further our proposal by considering other theoretical perspectives to judge how robust our ideas actually are.

II. MODEL SYSTEM AND METHOD

To verify the two proposals for the EB effect discussed above, here an approach complementary to that followed in the original publication Ref. 22 will be pursued, namely the *ab-initio* density-functional theory (DFT) simulation will be employed. It should be remarked that although the DFT methods are becoming more and more powerful in several branches of condensed matter physics and materials science, it is rare to find DFT applications in the field of exchange bias. The reason is that in most previous scenarios proposed to understand the EB effect, large length scales are involved, and the phenomenon is described as induced by magnetic domains and metastable states. These subtle effects are believed to be beyond the ability of current DFT techniques. However, the two mechanisms proposed in Ref. 22 are intrinsic and they are supposed to occur at the atomic scale, which allows to investigate their existence employing a DFT methodology.

In this publication, the model system is chosen to be a $SrRuO_3/SrMnO_3$ superlattice. This system is ideal for our purposes for several reasons: (1) It has been known from experiments that the Mn spins lie in-plane and form a G-type AFM order while the Ru spins point out-of-plane and form a FM order;[32–36] (2) All layers (SrO, RuO_2, MnO_2) are non-polar, which excludes the possible transfer of charge due to the polar catastrophe. Since it is expected that the Fermi energy of metallic $SrRuO_3$ lies within the gap band of insulating $SrMnO_3$, then charge transfer due to different work functions are not expected to be of relevance either; (3) The A-site cations are both Sr^{2+}, which provides a unique interfacial termination. And the EB has indeed been observed experimentally in these superlattices.[32–36]

The DFT calculations were here performed based on the projected augmented wave (PAW)[37] pseudopotentials using the Vienna *ab initio* Simulation Package (VASP).[38,39] The valence states include $4s4p5s$, $3p4s3d$, $4p5s4d$, and $2s2p$ for Sr, Mn, Ru, and O, respectively. The electron-electron interaction is described using the generalized gradient approximation (GGA) method.

A superlattice structure $(SrRuO_3)_2$-$(SrMnO_3)_2$ (totally 40 atoms) is stacked along the [001] axis, as shown in Fig. 2(a). The initial atomic positions are set as in the bulk arrangement for $SrRuO_3$ and the in-plane crystal lattice constants are set as 3.905 Å to match the widely-used $SrTiO_3$ substrate. Then, the out-of-plane lattice constant is relaxed. And the atomic positions of the superlattices are also fully optimized as the Hellman-Feynman forces are converged to less than 0.01 eV/Å. This optimization and electronic self-consistency are performed under a non-magnetic state.

After the optimization of the atomic positions, different magnetic profiles are applied into the system. The initial magnetic moments are ±3 for Mn (G-type AFM) and 2 for Ru (FM). The options in the codes to include the noncollinear spins and the SOC will be switched on or off in our investigations.

Due to its SOC origin, the DM interaction is quite weak, thus a high precision calculation is needed. In all the following calculations reported here, the PREC tag is set as ACCURATE. All calculations have been carried out using the plane-wave cutoff of 550 eV and a $9\times9\times3$ Monkhorst-Pack (MP) k-point grid in combination with the tetrahedron method.[40] These high energy cutoff and high MP k-grid make the present DFT calculations very CPU- and memory-demanding for the noncollinear spin states with SOC.

Even with the accuracy described above, the signals for a bias field remain very weak. Inspired by the differential circuit for weak signals methods, the DFT energies are here always compared in pairs to get the difference ΔE, a procedure that can considerably eliminate systematic inaccuracies during the calculation. In each pair, the FM moments of the $SrRuO_3$ layers are flipped by 180°, while all other inputs remain exactly the same. The energies before and after the spin flipping are compared to verify whether a bias exists. With these methods, the systematic fluctuations in our calculations can be suppressed below 1 meV or even lower.[41,42]

III. RESULTS AND DISCUSSION

The optimized lattice is shown in Fig. 2(a). When in the bulk, $SrMnO_3$ is cubic[43] while $SrRuO_3$ is orthorhombic.[44] Thus, the oxygen octahedral distortion in the $SrRuO_3$-$SrMnO_3$ superlattice (on $SrTiO_3$) is inherited from $SrRuO_3$. Here all Mn-O-Mn, Mn-O-Ru, and Ru-O-Ru bonds are bending: the in-plane bond angles are 176.3° for Mn-O-Mn and 156.2° for Ru-O-Ru; the out-of-plane bond angles are 173.8° for Mn-O-Mn, 167.7° for Ru-O-Ru, and 170.4° for Ru-O-Mn. It is clear that the bonds in $SrMnO_3$ are very close to straight while the bonds in $SrRuO_3$ are more bending, implying here that this bending of the bonds is due to $SrRuO_3$, in agreement with the arguments presented above. Here, the tilting angle of the octahedra in $SrRuO_3$ ($180-167.7=12.3°$) is close to, but slightly different, from the previous DFT result (10.5°) on a pure FM $SrRuO_3$ film on $SrTiO_3$.[45] Considering the differences between the studied systems and the differences in the details of the calculations, this observed nice agreement between our present results and the previous ones suggests that our approach is reasonable.

Let us consider first the collinear spin state without the SOC. The output local magnetic moments are 2.56 ± 0.05 μ_B for Mn and 1.42 ± 0.01 μ_B for Ru, which are close to the experimental data and to previous DFT calculations (with LSDA or LSDA+U) in the corresponding bulk materials.[46–48] These magnetic moments suggest the robust stability of the G-type AFM + FM spin configurations in the $(SrRuO_3)_2$-$(SrMnO_3)_2$ superlattice.[49] The weak disproportions (±0.05 for Mn and ±0.01 for Ru) arise from the different possible bonds (Mn(↑)-O-Ru(↑)

versus Mn(↓)-O-Ru(↑), where ↑ and ↓ denote the directions of the spins).

The energy difference (ΔE) is only 0.058 meV, which is already far below the expected precision of VASP, since even the default accuracy for electronic minimization is 0.1 meV in VASP. Thus, it is clear that these two states before and after the Ru's spin flipping must be degenerate, or in other words no bias effect is present. This degeneracy is certainly to be expected considering the presence of independent inversion symmetries in the spin space and crystal space.

A. DM driven EB

To verify the previously proposed DM-driven EB mechanism, the noncollinear spins are now considered. The initial spins of Ru ($\vec{S}_{\rm Ru}$) point out-of-plane while the spins of Mn ($\vec{S}_{\rm Mn}$) are in-plane, as observed in the real heterostructures.[32–36] Furthermore, the Mn spins are rotated within the $x-y$ plane for comparison.

At first, the SOC is kept "disabled" in the calculations (thus, no DM interaction is possible in principle). The ΔE's are 0.231 and 0.264 meV when $\vec{S}_{\rm Mn}$'s are along the x and y axes, 0.0016 and -0.023 meV when the $\vec{S}_{\rm Mn}$'s are along the two diagonal directions, and both 0.169 meV when the $\vec{S}_{\rm Mn}$'s are along (±2,±1,0) and (±2,∓1,0). These small ΔE's remain below the valid precision of VASP, implying again no bias effect. Thus, just having noncollinear spins is not sufficient to induce exchange bias.

Note that since the global breaking condition for the electronic self-consistent loop is 0.1 meV in the VASP package, the allowed error in the total energy is also of this magnitude. The observed small energy differences comparable to or below this threshold may originate from the self-consistent algorithm of VASP. These differences are smaller than the desired precision and they will not affect any physical conclusion. Only those energy differences larger than 1 meV (which is already a quite high precision for DFT) are considered to be physical in our calculations.

In the next step in our analysis, both the noncollinear spins and the SOC become "enabled" in the DFT calculation. The SOC will contribute to not only the site magnetocrystalline anisotropy but also the DM interaction. Now the energy differences ΔE's become quite nontrivial, since they depend on the spins' directions, as summarized in Tab. II.

By keeping the $\vec{S}_{\rm Ru}$ spins along the z-axis, the in-plane rotations of $\vec{S}_{\rm Mn}$'s give an isotropic trace: ΔE is 3.404 meV when $\vec{S}_{\rm Mn}$ is along the x-axis, and -4.224 meV when $\vec{S}_{\rm Mn}$ is along the y-axis. The absolute values of these two ΔE's are close since the effective precision of VASP is of the order of 1 meV. Ideally, these two values should be identical considering the in-plane 90° rotational symmetry. The observed small but non-negligible ΔE's are certainly not due to the inaccuracy in the calculations, which should be below 1 meV according to the estimations discussed before, but they arise from a bias field that originates in the SOC. Even more interestingly, ΔE reaches a maximum (absolute) value -10.125 meV when $\vec{S}_{\rm Mn}$ is along the [110]-direction but it is almost zero (0.339 meV) when $\vec{S}_{\rm Mn}$ is along the $[1\bar{1}0]$-direction in the pseudo-cubic frame. *This nontrivial behavior exactly agrees with the $\vec{D}$'s vector directions*, namely here the $\vec{D}$'s across the interfaces are along the $[1\bar{1}0]$ direction since the interfacial oxygens' (in-plane) displacement is along the [110] direction, as found from the optimized crystal struc-

TABLE I. DFT calculations with noncollinear spins but with the SOC disabled. The $\vec{S}_{\rm Mn}$ and $\vec{S}_{\rm Ru}$ vectors shown here are the *initial* magnetic moments which will be reduced to the self-consistent values: $\sim 2.5-2.6\ \mu_{\rm B}$ for Mn and $\sim 1.4\ \mu_{\rm B}$ for Ru along their initial directions. The small canting components are $\sim 0.2\ \mu_{\rm B}$ (out-of-plane) for $\vec{S}_{\rm Mn}$ and $\sim 0.1\ \mu_{\rm B}$ (in-plane) for $\vec{S}_{\rm Ru}$, as shown in Fig. 3(a).

$\vec{S}_{\rm Mn}$	$\vec{S}_{\rm Ru}$	ΔE(meV)
(±3,0,0)	(0,0,2)	0.231
(0,±3,0)	(0,0,2)	0.264
(±2,±2,0)	(0,0,2)	−0.023
(±2,∓2,0)	(0,0,2)	0.016
(±2,±1,0)	(0,0,2)	0.169
(±2,∓1,0)	(0,0,2)	0.169

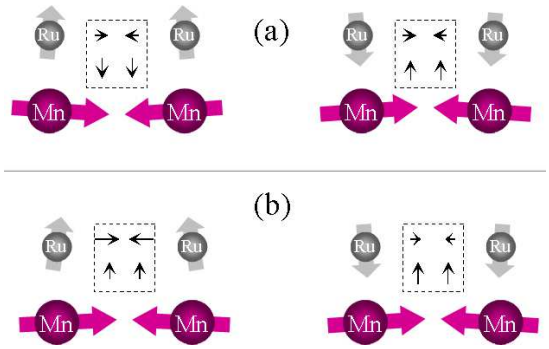

FIG. 3. (Color online) Sketches of interfacial noncollinear spin configurations after the self-consistency calculation reaches convergence. Here the initial spins $\vec{S}_{\rm Mn}$'s are along the (100) direction while $\vec{S}_{\rm Ru}$'s are along (001). All output spins show some canting, but small in value, from the initial axes. The canting components are shown in the insert boxes, where the lengths of arrows are in proportional to the values of canting momenta. (a) Results without SOC. The canting angles of $\vec{S}_{\rm Mn}$'s are about 4° while those of $\vec{S}_{\rm Ru}$'s are about 5°. After the flips of $\vec{S}_{\rm Ru}$'s (from left to right in the figure), all canting directions also flip symmetrically. (b) Results with SOC. The canting angles of $\vec{S}_{\rm Mn}$'s are about 3° (left) or 4° (right) while those of $\vec{S}_{\rm Ru}$'s are about 9° (left) or 4° (right). The canting angles (directions and values) are *no* longer symmetrical after the flips of $\vec{S}_{\rm Ru}$'s, which also suggests a bias due the SOC effect.

TABLE II. DFT calculations with the noncollinear spins and the SOC both enabled. The $\vec{S}_{\rm Mn}$ and $\vec{S}_{\rm Ru}$ are input magnetic moments. The output ones are $\sim$2.5$-$2.6 $\mu_{\rm B}$ for Mn and $\sim$ 1.4 $\mu_{\rm B}$ for Ru along their initial directions. For the first four cases, the observed small canting components are $\sim 0.1 - 0.2$ $\mu_{\rm B}$ (out-of-plane) for $\vec{S}_{\rm Mn}$ and $\sim 0.1 - 0.2$ $\mu_{\rm B}$ (in-plane) for $\vec{S}_{\rm Ru}$, as shown in Fig. 3(b). For the fifth case, the small canting components are < 0.1 $\mu_{\rm B}$ (out-of-plane) for $\vec{S}_{\rm Mn}$ and ~ 0.1 $\mu_{\rm B}$ (y-axis) for $\vec{S}_{\rm Ru}$. For the sixth case, the small canting components are $\sim 0.1 - 0.2$ $\mu_{\rm B}$ (y-axis) for $\vec{S}_{\rm Mn}$ and $\sim 0.1 - 0.2$ $\mu_{\rm B}$ (x-axis) for $\vec{S}_{\rm Ru}$.

$\vec{S}_{\rm Mn}$	$\vec{S}_{\rm Ru}$	ΔE(meV)
(±3,0,0)	(0,0,2)	3.404
(0,±3,0)	(0,0,2)	−4.224
(±2,±2,0)	(0,0,2)	−10.125
(±2,∓2,0)	(0,0,2)	0.339
(±3,0,0)	(2,0,0)	−0.272
(±3,0,0)	(0,2,0)	−0.311

ture. Note that since $SrRuO_3$ is a FM metal with itinerant magnetic moments, the DM formula $\vec{D} \cdot (\vec{S}_{\rm Ru} \times \vec{S}_{\rm Mn})$ which is based on localized moments may be inaccurate quantitatively. Even though, our DFT results confirm a qualitative agreement with DM ideas from the anisotropy of ΔE.

To further confirm the presence of a DM contribution, the $\vec{S}_{\rm Ru}$ spins are also initialized to be in-plane. However, in this case ΔE is almost zero no matter whether $\vec{S}_{\rm Ru} || \vec{S}_{\rm Mn}$ or $\vec{S}_{\rm Ru} \perp \vec{S}_{\rm Mn}$, as shown in the last two lines of Tab. II. Thus, all these DFT data provide clear qualitative evidence that the bias field is in the form of $\vec{D} \cdot (\vec{S}_{\rm Mn} \times \vec{S}_{Ru})$ and $\vec{D}$ is along the $[1\bar{1}0]$ direction of the pseudo-cubic frame.

The maximum value of the bias field driven by the DM interaction is found to be about 2.5 meV per Mn-O-Ru bond (here totally four Mn-O-Ru bonds across two interfaces due to the periodic boundary conditions), which is *larger* than our previous estimation[22] by two orders of magnitude. There are two reasons for finding such a prominent bias field. The most important one is that in our previous estimation a very small bond bending (= 1°) was assumed, which was clearly an underestimation for the present $(SrRuO_3)_2/(SrMnO_3)_2$ case ($\approx 10°$, as shown in Fig. 2(b)). Another possible reason for the discrepancy may be induced by the Ru cations because the SOC of the 4*d* electrons is much stronger than for the 3*d* ones. In any case, regardless of the actual reasons for the discrepancies in the estimations, finding a stronger effect than previously predicted only makes our proposals to understand the EB effect more robust.

TABLE III. DFT calculations with interfacial FE polarizations. Here only collinear spins are considered, namely the SOC is disabled. The $S_{\rm Mn}$ and $S_{\rm Ru}$ are input magnetic moments. The output ones are $\sim 2.5 - 2.6$ $\mu_{\rm B}$ for Mn and $\sim$ 1.4 $\mu_{\rm B}$ for Ru.

$S_{\rm Mn}$	$S_{\rm Ru}$	$\delta\vec{r}$ (Å)	ΔE (meV)
±3	2	(0.005,0.005,0)	16.307
±3	2	(−0.005,−0.005,0)	−16.486

B. FE driven EB

To fully verify our previous proposals, it is now necessary to check the bias field that is driven by the FE polarizations. However, here neither $SrRuO_3$ nor $SrMnO_3$ is a FE material. Then, to test this FE mechanism it is necessary to apply an "artificial" polarization at the interfaces. For this purpose, the oxygen anions between Ru and Mn are slightly displaced ($\delta\vec{r}$) uniformly from its optimized position to mimic an in-plane polarization.[50] These displacements provide modulated Ru-O-Mn bonds ($\gamma = 171.6°$ and $\beta = 168.5°$ when $\delta\vec{r} = (0.005, 0.005, 0)$Å, while the original one is $\alpha = 170.4°$), as shown in Figs. 2(b), (c), and (d)). Although these displacements are imposed manually, their result, namely the presence of modulated bonds, had already been confirmed in our previous DFT optimized analysis of $La_{3/4}Sr_{1/4}MnO_3/BiFeO_3$ superlattices since $BiFeO_3$ is a multiferroic material (for more details, see the supplementary material of Ref. 22). Since the proposed FE-driven EB does not require noncollinear spin configurations, here only collinear patterns are considered and the SOC is disabled. The results are summarized in Tab. III.

From the results shown above, it is obvious that the in-plane FE polarization at interfaces can indeed induce an EB field via the modulation of normal exchanges (note that the total effect on the DM interaction from such a bond angle modulation will be cancelled at the first order approximation, and thus can be neglected especially when the weak intensity of the DM interaction is considered). The bias field is about 4 meV per Ru-O-Mn bond and the FE polarization corresponding to $|\delta\vec{r}| = 0.005\sqrt{2}$ Å is about 3.5 mC/m^2. Although to be expected, it is very interesting to note that this EB field can be switched between positive and negative values by flipping the FE polarization using electrical methods, which can provide hints to understand the interfacial magnetoelectricity in $BiFeO_3$-based multiferroic heterostructures.[15,20,21]

It should be pointed out that the exchange striction effect could also induce such a modulation of the bond angles, namely the bond angle between a parallel spins' pair is different from that between an antiparallel spins' pair, e.g. in the multiferroic orthorhombic $HoMnO_3$,[51,52] which is driven by the non-relativistic exchange (J) between spins. This bond modulation can be easily observed if the lattice is optimized under a collinear G-AFM

plus FM configuration: the Ru(↑)-O-Mn(↑) (or Ru(↓)-O-Mn(↓)) becomes 164.5° while the Ru(↑)-O-Mn(↓) (or Ru(↓)-O-Mn(↑)) becomes 168.3°. However, in principle, this bond modulation would be switched following the switching of FM moments, implying the absence of a bias effect although the coercive field might be increased. Thus, only the FE polarization can give rise to a robust bond modulation with an origin independent of the exchange striction. Of course, the (inverse effect of) exchange striction can affect the underlying FE polarization when switching the FM moments, which is also an important issue for interfacial magnetoelectricity.

IV. CONCLUSION

Summaryzing, in this investigation the *ab initio* method has been used to verify previous proposals that were presented to rationalized the exchange bias effect in compensated antiferromagnets. The DFT calculation discussed here indeed provides qualitative evidence that both the Dzyaloshinskii-Moriya interaction and the ferroelectric polarization can induce exchange bias effects in perovskites heterostructures. Their common ingredient is the intrinsic bending of the bonds across the interface, which is induced by the oxygen octahedra rotations and tiltings. It can be argued that the proposed mechanisms originate from "uncompensated exchanges", namely the exchanges ($\vec{D}$ and J) are no longer uniform but modulated following the period of the antiferromagnetic order. The "uncompensated exchanges" emphasized in this work have usually been ignored in the previous models for the EB effect that mainly rely on uncompensated moments at the AFM interfaces.

V. ACKNOWLEDGMENTS

S.D. and J.M.L were supported by the 973 Projects of China (2011CB922101, 2009CB623303), NSFC (11004027), and NCET (10-0325). Q.F.Z and S.Y were supported by CREST-JST. E.D. was supported by the U.S. Department of Energy, Office of Basic Energy Sciences, Materials Sciences and Engineering Division. Most calculations were performed on the Kraken (a Cray XT5) supercomputer at the National Institute for Computational Sciences (`http://www.nics.tennessee.edu/`).

[1] J. Nogués and I. K. Schuller, J. Magn. Magn. Mater. **192**, 203 (1999).
[2] J. Nogués, J. Sort, V. Langlais, V. Skumryev, S. Suriñach, J. S. Muñoz, and M. D. Baró, Phys. Rep. **422**, 65 (2005).
[3] R. L. Stamps, J. Phys. D: Appl. Phys. **33**, R247 (2000).
[4] A. E. Berkowitz and K. Takano, J. Magn. Magn. Mater. **200**, 552 (1999).
[5] Y. Ijiri, J. Phys.: Condens. Matter **14**, R947 (2002).
[6] S. Giri, M. Patra, and S. Majumdar, J. Phys.: Condens. Matter **23**, 073201 (2011).
[7] M. Kiwi, J. Magn. Magn. Mater. **234**, 584 (2001).
[8] A. P. Malozemoff, Phys. Rev. B **35**, R3679 (1987).
[9] T. C. Schulthess and W. H. Butler, Phys. Rev. Lett. **81**, 4516 (1998).
[10] N. C. Koon, Phys. Rev. Lett. **78**, 4865 (1997).
[11] M. D. Stiles and R. D. McMichael, Phys. Rev. B **59**, 3722 (1999).
[12] M. Kiwi, J. Mejía-López, R. D. Portugal, and R. Ramírez, Appl. Phys. Lett. **75**, 3995 (1999).
[13] L. W. Martin, Y.-H. Chu, and R. Ramesh, Mater. Sci. Eng. R **68**, 89 (2010).
[14] M. Bibes, J. E. Villegas, and A. Barthélémy, Adv. Phys. **60**, 5 (2011).
[15] Y.-H. Chu, L. W. Martin, M. B. Holcomb, M. Gajek, S.-J. Han, Q. He, N. Balke, C.-H. Yang, D. Lee, W. Hu, et al., Nature Mater. **7**, 478 (2008).
[16] L. W. Martin, Y.-H. Chu, M. B. Holcomb, M. Huijben, P. Yu, S.-J. Han, D. Lee, S. X. Wang, and R. Ramesh, Nano Lett. **8**, 2050 (2008).
[17] H. Béa, M. Bibes, S. Cherifi, F. Nolting, B. Warot-Fonrose, S. Fusil, G. Herranz, C. Deranlot, E. Jacquet, K. Bouzehouane, et al., Appl. Phys. Lett. **89**, 242114 (2006).
[18] J. Dho, X. Qi, H. Kim, J. L. MacManus-Driscoll, and M. G. Blamire, Adv. Mater. **18**, 1445 (2006).
[19] H. Béa, M. Bibes, F. Ott, B. Dupé, X.-H. Zhu, S. Petit, S. Fusil, C. Deranlot, K. Bouzehouane, and A. Barthélémy, Phys. Rev. Lett. **100**, 017204 (2008).
[20] P. Yu, J.-S. Lee, S. Okamoto, M. D. Rossell, M. Huijben, C.-H. Yang, Q. He, J. X. Zhang, S. Yang, M. J. Lee, et al., Phys. Rev. Lett. **105**, 027201 (2010).
[21] S. W. Wu, S. A. Cybart, P. Yu, M. D. Rossell, J. X. Zhang, R. Ramesh, and R. C. Dynes, Nature Mater. **9**, 756 (2010).
[22] S. Dong, K. Yamauchi, S. Yunoki, R. Yu, S. Liang, A. Moreo, J.-M. Liu, S. Picozzi, and E. Dagotto, Phys. Rev. Lett. **103**, 127201 (2009).
[23] I. Dzyaloshinsky, J. Phys. Chem. Solids **4**, 241 (1958).
[24] T. Moriya, Phys. Rev. **120**, 91 (1960).
[25] I. A. Sergienko and E. Dagotto, Phys. Rev. B **73**, 094434 (2006).
[26] J. B. Goodenough and J.-S. Zhou, J. Mater. Chem. **17**, 2394 (2007).
[27] S. J. May, J.-W. Kim, J. M. Rondinelli, E. Karapetrova, N. A. Spaldin, A. Bhattacharya1, and P. J. Ryan, Phys. Rev. B **82**, 014110 (2010).
[28] S. J. May, C. R. Smith, J.-W. Kim, E. Karapetrova, A. Bhattacharya1, and P. J. Ryan, Phys. Rev. B **83**, 153411 (2011).
[29] J. M. Rondinelli and N. A. Spaldin, Phys. Rev. B **82**, 113402 (2010).
[30] J. M. Rondinelli and N. A. Spaldin, Adv. Mater. **23**, 3363 (2011).
[31] K. Momma and F. Izumi, J. Appl. Crystallogr. **41**, 653C658 (2008).
[32] Y. Choi, Y. Z. Yoo, O. Chmaissem, A. Ullah, S. Kolesnik, C. W. Kimball, D. Haskel, J. S. Jiang, and S. D. Bader,

Appl. Phys. Lett. **91**, 022503 (2007).
[33] Y. Choi, Y. C. Tseng, D. Haskel, D. E. Brown, D. Danaher, and O. Chmaissem, Appl. Phys. Lett. **93**, 192509 (2008).
[34] Y. Choi, Y. Z. Yoo, O. Chmaissem, A. Ullah, S. Kolesnik, C. W. Kimball, D. Haskel, J. S. Jiang, and S. D. Bader, J. Appl. Phys. **103**, 07B517 (2008).
[35] P. Padhan and W. Prellier, Appl. Phys. Lett. **88**, 263114 (2006).
[36] P. Padhan and W. Prellier, Phys. Rev. B **72**, 104416 (2005).
[37] P. E. Blöchl, Phys. Rev. B **50**, 17953 (1994).
[38] G. Kresse and J. Hafner, Phys. Rev. B **47**, 558 (1993).
[39] G. Kresse and J. Furthmüller, Phys. Rev. B **54**, 11169 (1996).
[40] P. E. Blöchl, O. Jepsen, and O. K. Andersen, Phys. Rev. B **49**, 16223 (1994).
[41] P. Błoński and J. Hafner, Phys. Rev. B **79**, 224418 (2009).
[42] P. Błoński and J. Hafner, J. Phys.: Condens. Matter **21**, 426001 (2009).
[43] O. Chmaissem, B. Dabrowski, S. Kolesnik, J. Mais, D. E. Brown, R. Kruk, P. Prior, B. Pyles, and J. D. Jorgensen, Phys. Rev. B **64**, 134412 (2001).
[44] C. Jones, P. D. Battle, and P. Lightfoot, Acta Cryst. C: Cryst. Struct. Commun. **45**, 365 (1989).
[45] T. Zayak, X. Huang, J. B. Neaton, and K. M. Rabe, Phys. Rev. B **74**, 094104 (2006).
[46] T. Takeda and S. Ohara, J. Phys. Soc. Jpn. **37**, 275 (1974).
[47] J. M. Rondinelli, N. M. Caffrey, S. Sanvito, and N. A. Spaldin, Phys. Rev. B **78**, 155107 (2008).
[48] J. H. Lee and K. M. Rabe, Phys. Rev. Lett. **104**, 207204 (2010).
[49] Many spin configurations, including (1) full FM; (2) full G-type AFM; (3) full A-type AFM; (4) full C-type AFM; (5) C-type AFM (Mn) + A-type AFM (Ru); (6) C-type AFM (Mn) + FM (Ru); (7) G-type AFM (Mn) + A-type (Ru), have been tested, all of which have higher energies than the G-type AFM (Mn) + FM (Ru) configuration. However, an A-type AFM (Mn) + FM (Ru) configuration has even lower energy. This is due to the strong Ru-O-Mn exchange coupling because here the $SrMnO_3$ portion is too thin: two Ru-Mn interfaces for two Mn layers. In real heterostructures, the magnetic moments in $SrMnO_3$ are indeed canting from the ideal G-type AFM when there are only two Mn layers,[33] but this arrangement will return to the G-type AFM state when $SrMnO_3$ is thick enough. Even with these caveats, since a G-type AFM + FM configuration can be stabilized in the model system, the conclusion of our proof-of-principle calculations will not be affected qualitatively.
[50] Due to the two interfaces arising from the periodic boundary conditions, the displacements of oxygens at the upper and lower interfaces should be opposite.
[51] I. A. Sergienko, C. Şen, and E. Dagotto, Phys. Rev. Lett. **97**, 227204 (2006).
[52] S. Picozzi, K. Yamauchi, B. Sanyal, I. A. Sergienko, and E. Dagotto, Phys. Rev. Lett. **99**, 227201 (2007).